Journal of Power Sources 186 (2009) 528–531

Contents lists available at ScienceDirect

Journal of Power Sources

journal homepage: www.elsevier.com/locate/jpowsour

Short communication

A discussion on decay of discharge capacity for amorphous Mg–Ni–Nd hydrogen storage alloy

G.Y. Liang[a,*], D.C. Wu[a], Lu Li[a], L.J. Huang[b]

[a] Department of Material Physics, Science School, State Key Laboratory of Mechanical Behavior for Material, Xi'an Jiaotong University, Xi'an 710049, China
[b] Department of Chemical and Environmental Engineering, Qingdao University, Qingdao 266071, China

ARTICLE INFO

Article history:
Received 26 April 2008
Received in revised form 17 August 2008
Accepted 27 August 2008
Available online 3 September 2008

Keywords:
Amorphous alloy
Microstructure
Hydrogenation
Discharge capacity

ABSTRACT

Amorphous Mg–Ni–Nd alloys were prepared by melt-spun technique and their discharge capacity was measured. Microstructure of amorphous ribbons after different charge–discharge cycles was observed using high-resolution transmission electron microscopy (HRTEM), X-ray diffraction (XRD) and selected area electron diffraction (SAED). The structure evolution of amorphous $(Mg_{60}Ni_{25})_{90}Nd_{10}$ alloy during the charge–discharge cycles was investigated in detail. Experimental results showed that the structure evolution of amorphous ribbon was responsible for the decay of discharge capacity. During the charge–discharge cycles of amorphous $(Mg_{60}Ni_{25})_{90}Nd_{10}$ alloy, $NdMg_2Ni_9$ phase appeared after four cycles and Mg_2Ni phase appeared after six cycles. After 20 cycles the stable phases Mg_2Ni, α-Mg and Nd_2H_5 were present and the former $NdMg_2Ni_9$ phase disappeared. With crystallization of amorphous ribbon, the discharge capacity of amorphous $(Mg_{60}Ni_{25})_{90}Nd_{10}$ alloy dropped off. After 10 cycles the curve of discharge capacity tended to be smooth.

1. Introduction

Mg-based hydrogen storage alloys are considered as one of the most promising candidates for the 3rd generation alloys, because of their high discharge capacity, lower density and rich natural resources [1,2]. However, the practical application of Mg-based alloys is restrained by their poor hydriding–dehydriding kinetics at room temperature and their poor charge–discharge cycle stability. In order to improve hydriding–dehydriding kinetics of Mg-based alloys, the electrode materials of nanocrystalline and amorphous structures are investigated, which achieves a quite high discharge capacity at room temperature [3–7].

A common recognition has been made by many researchers that the decay of discharge capacity for Mg-based hydrogen storage alloys is mainly caused by two reasons, i.e. the corrosion of alloy in alkaline solution and the pulverization of alloy particles during charge–discharge cycles. However, unlike crystalline alloys, amorphous alloys have good resistance for corrosion and pulverization [8–10] because of the absence of any conventional grains and grain boundaries and the continuous volume change when H atoms get in and out the alloy particles. Thus, it is worthwhile to find another reason for the decay of amorphous alloys.

The aim of this paper is to give an investigation on the reason for the discharge capacity decay of amorphous Mg–Ni–Nd alloy caused by the microstructure transformation during the process of hydrogenation–dehydrogenation.

2. Experimental

Mg–Ni–Nd alloy ingots were prepared by melting a mixture of pure Nd metal and Mg–Ni intermediate alloy in a vacuum induction furnace under the protection of argon gas. Because of the low melting point and the high vapor pressure of Mg, a special melting technique, that is positive pressure protection and repeated melting, has to be taken to prevent serious evaporation of Mg and ensure composition homogeneity during preparation of master alloy ingot. The amorphous ribbons were produced by a single roller melt-spun technique (copper quenching disc with a diameter of 250 mm and surface velocity of about 39 ms^{-1}) in an argon atmosphere of 400 mbar. The ribbons were about 2 mm wide and 20-μm thick. The structure of Mg–Ni–Nd alloy samples fabricated by melt-spinning has been detected in our pervious work [4], as shown in Table 1.

In order to observe microstructure evolution during the charge–discharge process, the amorphous alloy ribbons were fixed in a special mold to form the negative electrode. The positive electrode was made of Ni–oxyhydroxide/dihydroxide. The alkaline solution was 6 mol L^{-1} KOH containing 20 g L^{-1} LiOH. The specimens were charged at 100 mA g^{-1} for 12 h and discharged at

* Corresponding author. Tel.: +86 29 82663747; fax: +86 29 83207910.
E-mail address: gyliang@mail.xtu.edu.cn (G.Y. Liang).

0378-7753/$ – see front matter © 2008 Published by Elsevier B.V.
doi:10.1016/j.jpowsour.2008.08.080

Table 1
The composition and structure of Mg-based alloy sample after melt-spinning

Sample no.	Composition	Microstructure
A	$(Mg_{60}Ni_{25})_{98}Nd_2$	Nanocrystalline
B	$(Mg_{60}Ni_{25})_{95}Nd_5$	Nanocrystalline + amorphous
C	$(Mg_{60}Ni_{25})_{90}Nd_{10}$	Amorphous
D	$Mg_{60}Ni_{25}Nd_{15}$	Amorphous

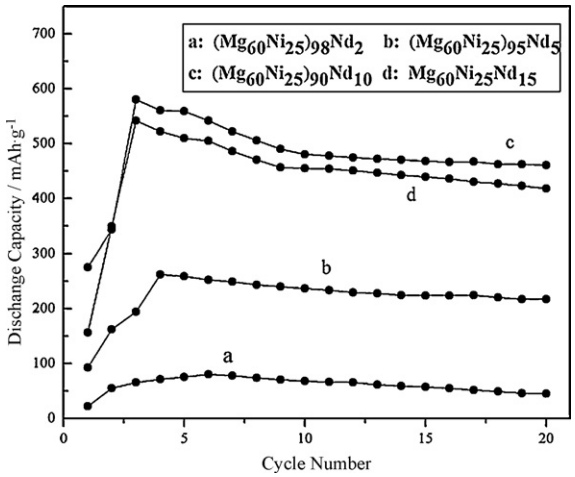

Fig. 1. Variation of the discharge capacity versus the cycle number for the different samples [4].

50 mA g^{-1} using the BT-2000 battery testing instrument (Arbin). The discharged cut-off potential was set to 0.8 V between the two electrodes. The resting time between the charge and discharge was 1 h.

The microstructure of the ribbons after charge–discharge cycles was examined by HRTEM (JEOL-2010) and XRD (Rjgaku D, Cu Kα).

3. Results

Fig. 1 shows the discharge capacity of different Mg–Ni–Nd alloys obtained in our prior study [4]. It is observed that the discharge capacity of amorphous samples is much higher than that of nano-crystalline samples, refer to Table 1. It is also found that the discharge capacity of amorphous $(Mg_{60}Ni_{25})_{90}Nd_{10}$ and $(Mg_{60}Ni_{25})_{85}Nd_{15}$ samples reaches a maximum at the 3rd cycle and then decreases during the future cycles.

Table 2 shows the capacity retention at the 10th cycle and 20th cycle for different samples. Although the amorphous samples can achieve quite high discharge capacity, the decay of discharge capacity is still significant. This phenomenon is much more obvious in other amorphous electrodes produced by high-energy milling [5,11].

Fig. 2 shows the discharge curves of $(Mg_{60}Ni_{25})_{90}Nd_{10}$ electrode at the 3rd, 4th, 6th, 10th, 15th and 20th cycles. The discharge potential increases with cycling. The rate of increase from the 3rd to 10th cycles is much larger than that of from the 10th to 20th cycles. Besides, the discharge potential plateau becomes more horizontal,

Table 2
The capacity retention of samples at the 10th cycle and 20th cycle

Samples	C_{max} (mAh g^{-1})	C_{10}/C_{max} (%)	C_{20}/C_{max} (%)
$(Mg_{60}Ni_{25})_{98}Nd_2$	80.2	85.0	56.8
$(Mg_{60}Ni_{25})_{95}Nd_5$	262.6	90.2	82.6
$(Mg_{60}Ni_{25})_{95}Nd_{10}$	580.5	82.7	80.4
$Mg_{60}Ni_{25}Nd_{15}$	541.8	83.9	77.1

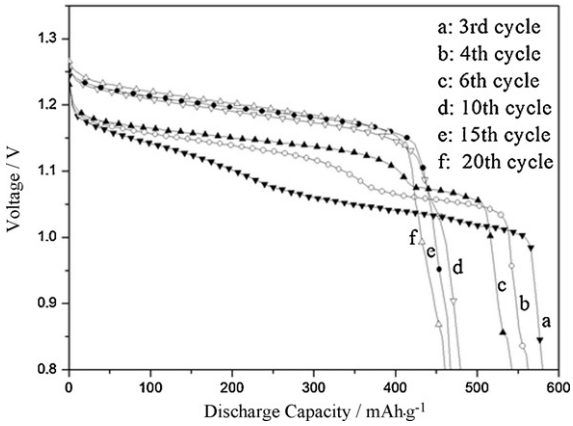

Fig. 2. The discharge voltage curves of $(Mg_{60}Ni_{25})_{90}Nd_{10}$ electrode at the: (a) 3rd, (b) 4th, (c) 6th, (d) 10th, (e) 15th and (f) 20th cycle.

which reveals the discharge potential characteristic is improving, but the discharge capacity is decreasing.

Fig. 3 shows XRD patterns of the amorphous $(Mg_{60}Ni_{25})_{90}Nd_{10}$ sample charged–discharged for 3, 4, 6, 10 and 20 cycles, respectively. The amorphous phase remains after three cycles, and gradually crystallizes during the future cycles. Nano-crystalline $NdMg_2Ni_9$ particles are detected in the 4th cycle (Fig. 3(b)), and nano-size Mg_2Ni appears in the 6th cycle (Fig. 3(c)). After 20 cycles some stable phases Mg_2Ni, α-Mg and Nd_2H_5 are present (Fig. 3(e)), and $NdMg_2Ni_9$ disappears.

Fig. 4 shows the HRTEM image and SAED pattern of amorphous $(Mg_{60}Ni_{25})_{90}Nd_{10}$ alloy charged–discharged for six cycles. It is found that nano-particles $NdMg_2Ni_9$ and Mg_2Ni are present. The size of $NdMg_2Ni_9$ particles is about 5–15 nm.

Fig. 5 shows the HRTEM image and SAED pattern of amorphous $(Mg_{60}Ni_{25})_{90}Nd_{10}$ alloy charged–discharged for 10 cycles. Nano-crystalline $NdMg_2Ni_9$ and Mg_2Ni particles are surrounded by the residual amorphous phase. In comparison with Fig. 4, it is found that $NdMg_2Ni_9$ and Mg_2Ni particles have grown up.

4. Discussion

During the first three cycles, the $(Mg_{60}Ni_{25})_{90}Nd_{10}$ sample undergoes an initial activation (Fig. 1(c)). The initial activation could be ascribed to the cracking of alloy particles during

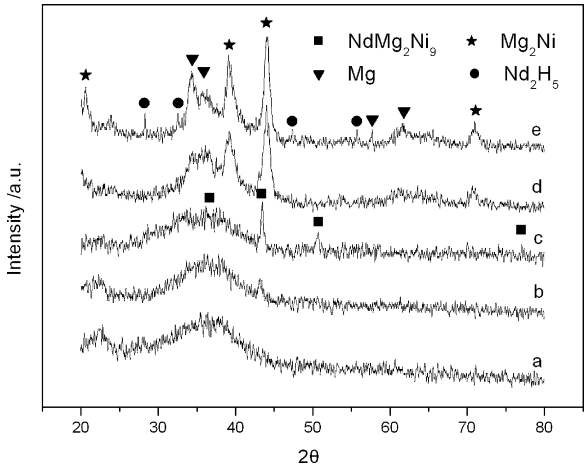

Fig. 3. XRD patterns of amorphous samples charged–discharged for: (a) three cycles, (b) four cycles, (c) six cycles, (d) 10 cycles and (e) 20 cycles, respectively.

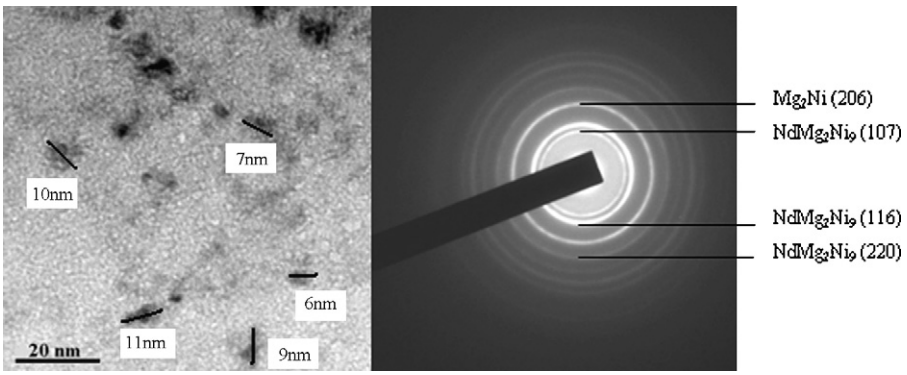

Fig. 4. HRTEM image and SAED pattern of amorphous $(Mg_{60}Ni_{25})_{90}Nd_{10}$ alloy charged–discharged for six cycles.

charge–discharge cycles. The cracking produces more fresh surfaces, and thus improves the discharge capacity. The amorphous structure of the $(Mg_{60}Ni_{25})_{90}Nd_{10}$ sample remains after three cycles (Fig. 3(a)). Concerning that the maximum discharge capacity appears at the 3rd cycle, it is obvious that the amorphous structure is beneficial to the absorption–desorption of hydrogen.

After three cycles, the discharge capacity begins to decay. Usually, the discharge capacity degradation of amorphous Mg-based hydrogen storage alloys is interpreted as the result of the corrosion of alloy in alkaline solution and the pulverization of alloy particles during charge–discharge cycles. However, it is found that the influence of the structural transformation of the alloy on the discharge capacity degradation is not negligible.

As shown in Fig. 1 and Table 2, the drop-off of discharge capacity could be divided into two steps according to the decay rate of discharge capacity, i.e. from the 3rd to the 10th cycles as the first step and from the 10th to the 20th cycles as the second step. The first step corresponds to the formation and the decomposition of $NdMg_2Ni_9$ as well as the formation of Mg_2Ni, while the second step corresponds to the presence of Mg_2Ni, α-Mg and Nd_2H_5 (Figs. 3–5). This indicates that $NdMg_2Ni_9$ leads to a faster decrease of the discharge capacity than Mg_2Ni, α-Mg and Nd_2H_5. Therefore, a conclusion could be drawn that the crystallization of amorphous $(Mg_{60}Ni_{25})_{90}Nd_{10}$ alloy is also responsible for the degradation of the discharge capacity.

The discharge potential of the $(Mg_{60}Ni_{25})_{90}Nd_{10}$ electrode increases with cycling, as shown in Fig. 2. This variety could be also divided into two steps according to the rate of increase, namely from the 3rd to 10th cycles as the first step and from 10th to 20th cycles as the second step. Combing with the structure transformation of the alloy, we believe the variety of the discharge potential is caused by the structure transformation. The fast increase of the discharge potential during 3–10 cycles is because the formation of $NdMg_2Ni_9$. When the stable Mg_2Ni, α-Mg and Nd_2H_5 are present in the alloy during 10–20 cycles, the increase of potential becomes slow. The formation of $NdMg_2Ni_9$ as well as Mg_2Ni, α-Mg and Nd_2H_5 improves the discharge potential characteristic of the electrode, but causes the decrease of discharge capacity.

During the charge process, great deals of H atoms get into the amorphous alloy and will bring microstress to the neighboring atoms, which may lead to nucleation in a very small region. This presumption is supported by the results reported by other scholars [12–14]. During the discharge process, H atoms get out and the previously formed crystal nuclei may decompose and the alloy structure turns back to amorphous state. However, some H atoms may be still in the alloy after discharge, and the remained nuclei will grow up during the further charge–discharge cycles.

Fig. 6 gives a simple illustration on how the crystallization of $(Mg_{60}Ni_{25})_{90}Nd_{10}$ affects the discharge capacity. Orimo and Fujii [15] reported that hydrogen concentration in amorphous region is 1.8 times than that in grain region of Mg_2Ni. The appearance of crystallites in the amorphous $(Mg_{60}Ni_{25})_{90}Nd_{10}$ alloy, as shown in Fig. 6, will take up the places which could hold more H atoms. Besides, the appearance of crystallites will also make the diffusion of H atoms more difficult. H atoms have to get round the crystallites, which induces long-range diffusion unavoidable. The two aspects discussed above might lead to the reduction of discharge capacity. Furthermore, the formation of crystal grains will accelerate the corrosion and pulverization of alloy, making the electrochemical properties worse. It is suggested that the over-discharge of the amorphous alloy is perhaps a way to restrain the growth of nuclei, and consequently lighten the degradation of the discharge capacity.

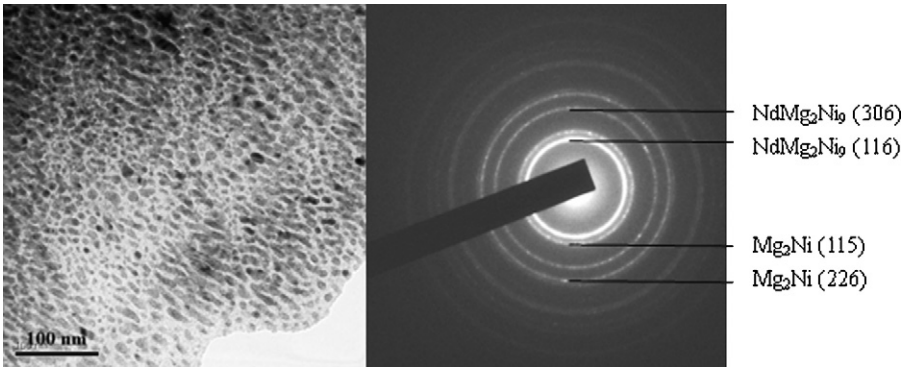

Fig. 5. HRTEM image and SAED pattern of amorphous $(Mg_{60}Ni_{25})_{90}Nd_{10}$ alloy charged–discharged for 10 cycles.

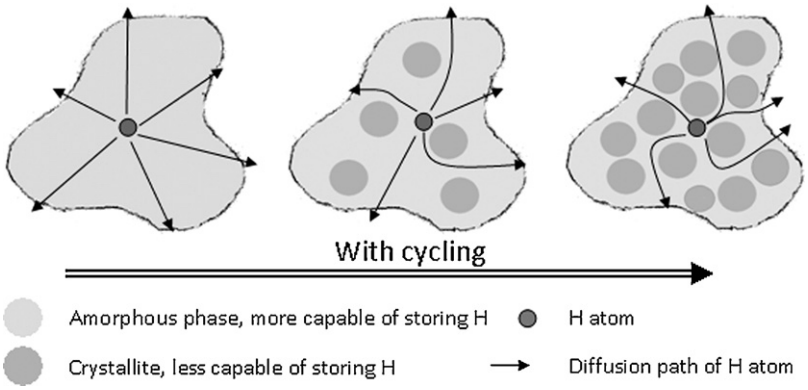

Fig. 6. A simple schematic explanation for the relationship between the crystallization of amorphous $(Mg_{60}Ni_{25})_{90}Nd_{10}$ alloy and the discharge capacity degradation with cycling.

5. Conclusion

The reason for the decay of discharge capacity of $(Mg_{60}Ni_{25})_{90}Nd_{10}$ alloy is discussed. It is found that the decrease of discharge capacity could be divided into two steps according to the decay rate of discharge capacity, i.e. from the 3rd to the 10th cycles as the first step and from the 10th to the 20th cycles as the second step. The first step corresponds to the formation and the decomposition of $NdMg_2Ni_9$ as well as the formation of Mg_2Ni, while the second step corresponds to the presence of Mg_2Ni, α-Mg and Nd_2H_5. It is indicated that the crystallization of amorphous $(Mg_{60}Ni_{25})_{90}Nd_{10}$ alloy is responsible for the decay of discharge capacity.

Acknowledgement

The project was supported by the State Key Development Program for Basic Research of China (Grant No. 2007CB707700).

References

[1] J.C. Bolcich, A.A. Yawuy, H.L. Corso, H.A. Pertti, C.O. Anala, Int. J. Hydrogen Energy 19 (1994) 605.
[2] L. Schlapbach, A. ZÜttel, Nature 414 (2001) 353.
[3] J.S. Xue, G.X. Li, Y.Q. Hu, J. Alloys Compd. 307 (2000) 240.
[4] L.J. Huang, G.Y. Liang, Z.B. Sun, D.C. Wu, J. Power Sources 160 (2006) 684.
[5] F.X. Wang, X.P. Gao, Z.W. Lu, J. Alloys Compd. 370 (2004) 326–330.
[6] M. Bououdina, D. Grant, G. Walker, Int. J. Hydrogen Energy 31 (2006) 177.
[7] L.J. Huang, G.Y. Liang, Z.B. Sun, J. Alloys Compd. 421 (2006) 279–282.
[8] J.W. Liu, L.F. Jiao, H.T. Yuan, Y.J. Wang, Q. Liu, J. Alloys Compd. 403 (2005) 270.
[9] B. Khorkounov, A. Gebert, C. Mickel, L. Schultz, J. Alloys Compd. 416 (2006) 110.
[10] X.Z. Xiao, X.H. Wang, L.H. Gao, W. Li, C.P. Chen, J. Alloys Compd. 413 (2006) 312.
[11] C. Rongeat, L. Roué, J. Power Sources 132 (2004) 302.
[12] P.R. Cha, Y.C. Kim, K.B. Kim, Scripta Mater. 56 (2007) 609.
[13] M.Q. Chandler, M.F. Horstemeyer, M.I. Baskes, Acta Mater. 56 (2008) 95.
[14] M.Q. Chandler, M.F. Horstemeyer, M.I. Baskes, Acta Mater. 56 (2008) 619.
[15] S. Orimo, H. Fujii, Appl. Phys. A 72 (2001) 167.